



Cite this: *CrystEngComm*, 2020, 22, 6347

# Polymorphism in 1-methylhydantoin: investigation by periodic DFT calculations and characterization of the third polymorph†

Bernardo A. Nogueira, <sup>\*ab</sup> Alberto Milani, <sup>b</sup> Gulce O. Ildiz, <sup>ac</sup> José A. Paixão, <sup>d</sup> Chiara Castiglioni <sup>b</sup> and Rui Fausto <sup>a</sup>

In previous studies [Puszyńska-Tuszkano *et al. Polyhedron*, 2011, **30**(12), 2016; Nogueira *et al. J. Phys. Chem. A*, 2014, **118**(31), 5994; Nogueira *et al. J. Mol. Struct.*, 2017, **1148**, 111], two different polymorphs of 1-methylhydantoin (1-MH, C<sub>4</sub>H<sub>6</sub>N<sub>2</sub>O<sub>2</sub>) were identified (forms I and II) and characterized using infrared and Raman spectroscopies, as well as by X-ray diffraction. In this work, a new polymorph of the compound (form III) is described. The new polymorph was characterized spectroscopically and its structure was determined for the first time by single crystal X-ray diffraction. Very interestingly, the crystal of polymorph III was found to exhibit a high-*Z'* (*Z'* = 3) asymmetric unit and 12 molecules in the unit cell (*Z* = 12), which contrasts with the simpler crystal structures found previously for forms I and II (*Z* = 4; *Z'* = 1). Besides, a thorough study of the polymorphism of 1-MH was performed with the help of state-of-the-art first principles fully periodic calculations of the structure, as well as infrared and Raman spectra of the different polymorphs of the compound. Marker-bands in the infrared and Raman spectra of the polymorphs are proposed for fast spectroscopic identification of the polymorphs.

Received 14th July 2020,  
Accepted 3rd September 2020

DOI: 10.1039/d0ce01016b

rsc.li/crystengcomm

## 1. Introduction

Polymorphism is the ability of a compound to exist in different crystallographic structures, resulting from different packing arrangements of its molecules in the crystal.<sup>1</sup> It is nowadays a very active subject of research due to its implications in many areas, in particular for the pharmaceutical industry, because different polymorphs of the same compound may exhibit substantially dissimilar physical and chemical properties, as well as pharmacokinetics, bioavailability and bioactivity in general.<sup>1,2</sup>

In the last few years, we have been developing a research program focused on polymorphism of hydantoins,<sup>3–10</sup> which are important biologically active compounds receiving many pharmaceutical uses, such as anticonvulsive, antiepileptic, anti-inflammatory and anti-cancer drugs;<sup>11–16</sup> some hydantoins have also been suggested to have anti HIV-1

activity.<sup>17</sup> In that research program we started to investigate the parent hydantoin compound,<sup>4,5</sup> and then some of its simpler derivatives, specifically 1-methylhydantoin (1-MH),<sup>6,7</sup> 5-methylhydantoin (5-MH),<sup>8</sup> and 5-acetic acid hydantoin and its sodium salt.<sup>9,10</sup> With exception of the parent compound, all the previously studied hydantoins share the common feature of exhibiting polymorphism.<sup>5–10</sup>

In the case of 1-MH (Fig. 1), we have reported on the structure, photochemistry and infrared spectra of the isolated molecule of the compound,<sup>6</sup> and described for the first time its second polymorph (form II).<sup>7</sup> The first known polymorph of 1-MH (form I) was reported in 2011 by Puszyńska-Tuszkano and co-workers.<sup>18</sup>

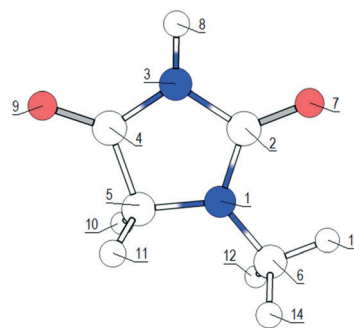


Fig. 1 Minimum energy structure of isolated 1-MH molecule, as predicted by DFT(B3LYP)/6-31G(d,p) calculations.

<sup>a</sup> CQC, Department of Chemistry, University of Coimbra, P-3004-535 Coimbra, Portugal. E-mail: ban@qui.uc.pt

<sup>b</sup> CMIC, Dipartimento di Chimica, Materiali e Ingegneria Chimica “G. Natta”, Politecnico di Milano, 20133, Milano, Italy

<sup>c</sup> Department of Physics, Faculty of Sciences and Letters, Istanbul Kultur University, 34158 Istanbul, Turkey

<sup>d</sup> CFisUC, Department of Physics, University of Coimbra, P-3004-516, Coimbra, Portugal

† Electronic supplementary information (ESI) available. CCDC 2010673. For ESI and crystallographic data in CIF or other electronic format see DOI: 10.1039/d0ce01016b

In this article, we report on a third polymorphic form (form **III**) of 1-MH. The new polymorph was synthesized by recrystallization from a diluted  $\text{MgCl}_2$  aqueous solution, and a suitable crystal was then used for single crystal X-ray diffraction structure determination. The crystal was found to exhibit a rare high- $Z'$  ( $Z' = 3$ ) asymmetric unit and 12 molecules in the unit cell ( $Z = 12$ ), which contrasts with the simpler crystal structures found previously for polymorphs **I** and **II** ( $Z = 4$ ;  $Z' = 1$ ).<sup>7,18</sup> The new material was also characterized by Raman spectroscopy. The experimental studies have been complemented by state-of-the-art fully periodic density functional theory (DFT) calculations.

Besides the structural and spectroscopic characterization of the new polymorph of 1-MH *per se*, the present study also compares the properties of this form with those of polymorphs **I** and **II** in order to characterize in a comparative basis, the dominant intermolecular interactions present in the different polymorphs.

## 2. Experimental and computational methods

### 2.1. Synthesis of the new polymorph

1-Methyldihydantoin was purchased from Sigma-Aldrich (98% purity). The crystal screening considered samples of the compound obtained by recrystallization, at room temperature, from aqueous solutions with different dissolved inorganic salts. Crystals of the new polymorph **III** were obtained by the recrystallization from an aqueous solution with dissolved magnesium chloride ( $\text{MgCl}_2$ ).

### 2.2. Raman spectroscopy

Raman spectra (1.5  $\text{cm}^{-1}$  resolution) were obtained in the wavenumber range 50–4000  $\text{cm}^{-1}$  with 633 nm HeNe laser excitation, using a Horiba LabRam HR Evolution Raman micro-system, equipped with a synapse CCD detector, a high-stability BXFM open space confocal microscope, and a 600  $\text{gr mm}^{-1}$  grating. The laser power at the sample was  $\sim 17$  mW, and the exposure time 30 seconds (accumulated 10 times). A 50 $\times$  objective lens was used, giving a laser spot diameter of 0.8  $\mu\text{m}$  at the sample.

### 2.3. X-ray crystallography

The X-ray diffraction data were collected in a Bruker APEXII diffractometer, at  $293 \pm 2$  K, using graphite monochromated  $\text{MoK}\alpha$  ( $\lambda = 0.71073$  Å) radiation. Data integration and scaling were performed with the SAINT suite of programs and absorption corrections were done using SADABS.<sup>19</sup>

The structure was solved by direct methods using SHELXT-2014/5.<sup>20</sup> Refinements were carried out with the SHELXL-2018/3 package<sup>21</sup> by full-matrix least-squares on  $F^2$ , with anisotropic displacement parameters for all non-hydrogen atoms (see ESI† – crystallographic tables, for details regarding the crystallographic analysis procedures and also for detailed crystal data). All hydrogen atoms could be

located on a difference Fourier synthesis; their positions were refined as riding on parent atoms with an isotropic temperature constrained to those of their parent atoms using SHELXL-2018/3 defaults,<sup>21</sup> except those attached to N atoms that are involved in hydrogen bonding, which had their positions freely refined.

A CIF file containing supplementary crystallographic data was deposited at the Cambridge Crystallographic Data Centre with reference CCDC 2010673.

### 2.4. Computational details

Full geometry optimization of the crystal structure and the prediction of infrared (IR) and Raman spectra of polymorphs **I**, **II** and **III** of 1-MH have been carried out using the CRYSTAL17 (ref. 22 and 23) code within the framework of the density functional theory (DFT). In order to test the accuracy of different functionals and basis sets, the B3LYP<sup>24,25</sup> and PBE0 (ref. 26) hybrid exchange–correlation functionals, and the 6-31G(d,p) and pob-TZVP<sup>27</sup> basis sets were used. The empirical correction for dispersion interaction (DFT-D) proposed by Grimme<sup>28–30</sup> was also applied in order to consider van der Waals and other dispersion attractive interaction forces. In all calculations, the atomic positions as well as the lattice parameters were fully optimized. The input structures for the calculations were the experimentally determined ones published by Puszyńska-Tuszkankow and co-workers,<sup>18</sup> and Nogueira *et al.*,<sup>7</sup> for forms **I** and **II**, respectively, and the structure reported in the present work for polymorph **III**.

Vibrational frequencies calculations at the  $\Gamma$  point have been done on the optimized geometries, as achieved by the diagonalization of the numerically calculated Hessian matrix. The predicted normal modes were included in the discussion presented in sections 3.5 and 3.6 if the predicted intensity was  $>5$   $\text{km mol}^{-1}$  in IR and  $>5$   $\text{Å}^4 \text{amu}^{-1}$  in Raman. All predicted frequencies were scaled by a single factor (0.9648) to allow a better comparison with the experimental data.

## 3. Results and discussion

### 3.1. Crystal structure of the new polymorph **III**

Polymorph **III** of 1-MH crystallizes in the orthorhombic Sohncke space group  $P2_12_12_1$  with cell parameters  $a = 7.8466(2)$ ,  $b = 9.8257(3)$ ,  $c = 20.3107(7)$  Å. The unit cell contains 12 molecules and the space-group has 4 symmetry operators, therefore the asymmetric unit contain 3 non-symmetry related molecules ( $Z' = 3$ ), which are depicted in Fig. 2.

The packing of the molecules in the crystal results in a layered structure (Fig. 3), the layers being parallel to the  $ab$  plane and stacked along the  $c$ -axis, with the spacing between the layers being approximately one sixth of the  $c$ -axis length (3.39 Å).

There are two distinct type of layers, those formed only by A molecules (layers located at  $z = 0$  and  $z = 1/2$ ) and those formed by B and C molecules (layers located at  $z = 1/6, 2/6, 4/$

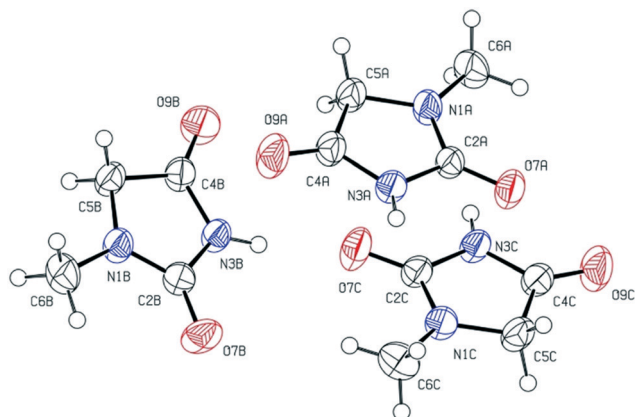


Fig. 2 ORTEP plot showing the anisotropic displacement ellipsoids and atom numbering scheme for the 3 molecules present in the asymmetric unit of the crystal structure of polymorph III of 1-MH. The ellipsoids are drawn at the 50% probability level.

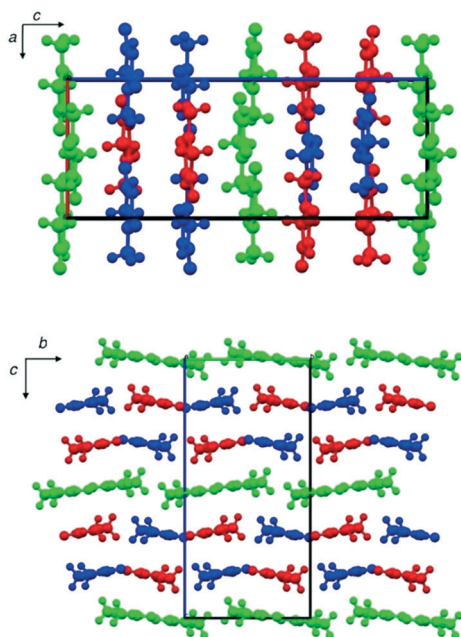


Fig. 3 Projection of the structure of polymorph III along the crystallographic *b*- (top panel) and *a*- (bottom) axis. Molecules A, B and C are depicted in green, red and blue, respectively.

6 and 5/6). The layer stacking is thus A, B + C, B + C, A, ... along the *c*-axis. Each of these layers is formed by chains of molecules joined by N-H...O hydrogen bonds running along [100], parallel to the shortest crystallographic axis. These chains are disjoint, as no strong hydrogen bond interactions connect the chains, only weaker C-H...O and possibly  $\pi\cdots\pi$  and C-O... $\pi$  interactions involving the electron clouds of the hydantoin rings.

The hydrogen bonding motif is similar in the two types of layers (Fig. 4), the N-H groups acting as proton donors towards the O7 atoms, which act as acceptors. In the B + C type of layers, two distinct N-H...O bonds are present, one where the N3B atom donates the proton to the O7C atom,

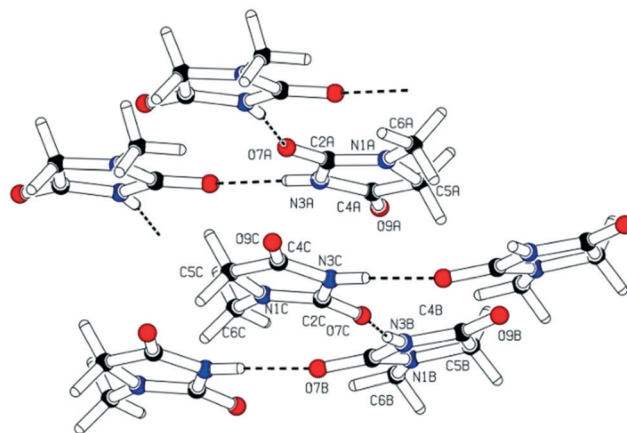


Fig. 4 N-H...O hydrogen-bonding patterns in the A-type and B + C-type chain of molecules.

and the other with the N3C atom being the donor and the O7B the acceptor. In the A-type layer, only one type of hydrogen bonding is present. Details of the hydrogen-bond interactions are given in Table 1. One can see that the N-H...O hydrogen bonds are strong with a  $^{\circ}\text{N-H}\cdots\text{O}$  angle close to linear geometry, as expected. The observed N...O distances range between 2.792(2) and 2.828(2) Å, the spread of distances being small but significant. In addition, short intermolecular contacts exist between the H atoms bound to C5 and the O9 atom of neighbour molecules, one of these contacts being established between chains of the B + C layers and the other two in the A layers.

### 3.2. Comparison of the crystal structures of the three polymorphs of 1-MH

The previously known polymorphs of 1-MH crystallize in the monoclinic system with space-group  $P2_1/c$  (form I) and in the orthorhombic system with space group  $Pna2_1$  (form II).<sup>13,14</sup> In both cases, and in contrast with the new polymorph III, there is only one symmetry independent molecule ( $Z' = 1$ ) and only 4 molecules in the unit cell ( $Z = 4$ ). Interestingly, the structures of polymorphs II and III are acentric, whereas that of polymorph I is centric. A summary

Table 1 Details of the hydrogen-bonding interactions and short and C-H...O intermolecular contacts<sup>a</sup>

D-H...A	D-H	H...A	D...A	$\angle\text{D-H}\cdots\text{A}$
N3-H8A...O7A(i)	0.80(3)	2.03(3)	2.822(2)	172(3)
N3B-H8B...O7C	0.86(3)	1.94(3)	2.792(2)	171(3)
N3-H8C...O7B(ii)	0.84(3)	1.99(3)	2.828(2)	176(2)
C5A-H11A...O9A(iii)	0.97	2.46	3.228(3)	136
C5B-H11B...O7B(iv)	0.97	2.49	3.410(3)	158
C5C-H10C...O9B(v)	0.97	2.59	3.185(3)	120

<sup>a</sup> Distances and angles are given in Å and  $^{\circ}$ , respectively. D and A represent hydrogen bond donors and acceptor atoms, respectively. Symmetry codes: (i)  $-1/2 + x, 1/2 - y, 1 - z$ ; (ii)  $1 + x, y, z$ ; (iii)  $1/2 + x, 3/2 - y, 1 - z$ ; (iv)  $-x, 1/2 + y, 1/2 - z$ ; (v)  $x, -1 + y, z$ .

**Table 2** Crystallographic data for the three polymorphs of 1-MH, resolved at 25 °C<sup>a</sup>

	Polymorph I	Polymorph II	Polymorph III
<i>a</i>	5.601(10)	19.0258(4)	7.8466(2)
<i>b</i>	12.178(3)	3.91210(10)	9.8257(3)
<i>c</i>	8.090(2)	6.82880(10)	20.3107(7)
$\alpha$	90	90	90
$\beta$	105.62(2)	90	90
$\gamma$	90	90	90
Volume	531.4(2)	508.273(18)	1565.92(8)
Space group	<i>P</i> 2 <sub>1</sub> / <i>c</i>	<i>Pna</i> 2 <sub>1</sub>	<i>P</i> 2 <sub>1</sub> 2 <sub>1</sub> 2 <sub>1</sub>
<i>Z</i>	4	4	12
<i>Z'</i>	1	1	3
<i>D</i> <sub>calc</sub>	1.426	1.491	1.452

<sup>a</sup> Values of *a*, *b* and *c* are in Å,  $\beta$  in degrees, volume in Å<sup>3</sup>, and density (*D*<sub>calc</sub>) in g cm<sup>-3</sup>.

of crystallographic data for the three forms is provided in Table 2.

Being a rigid molecule, the conformation of the 1-MH molecule is identical in all polymorphs, but the three forms show considerably distinct intermolecular interactions, as determined by the different molecular packing. In form **I** strong N3–H⋯O7 bond interactions ( $d(\text{N3}\cdots\text{O7}) = 2.8148(17)$  Å;  $\angle(\text{N3-H}\cdots\text{O7}) = 173.5(16)^\circ$ )<sup>18</sup> group the molecules in dimers (pairs of molecules related by an inversion center), which are then associated in chains by weaker non-conventional C5–H⋯O7 interactions (Fig. 5a). The main hydrogen-bonding pattern in polymorph **II** is more similar to that of polymorph **III**, since like in this latter form, it consists of chains of molecules linked by N3–H⋯O7 interactions. However, the way these chains of molecules pack in the crystal is strikingly different in polymorphs **II** and **III**. In form **III** the chains pack in parallel layers stacked along the *c*-axis, as described in the previous section, while in polymorph **II** zigzag chains of molecules are interspersed with other chains through weak C5–H10⋯O9 and C5–H11⋯O9 interactions in such a way that they form an angle of *ca.* 36° with each other (Fig. 5b). In this form, the N3–H⋯O7 H-bond distance is  $d(\text{N3}\cdots\text{O7}) = 2.817(2)$  Å,<sup>7</sup> *i.e.*, slightly shorter than in the new polymorph **III**.

The densities of the three polymorphs follow the order **I** < **III** < **II**, in consonance with the corresponding unit cell volumes (in the case of form **III**, 1/3 of the unit cell volume, 521.97 Å<sup>3</sup>), very interestingly the same order as the relative energies of the crystals of the polymorphs, as predicted by the DFT calculations presented in section 3.4. Though the reasons for the relative energies of the crystals of the three 1-MH forms are certainly a result of several factors, the fact that they correlate inversely with the densities points to the relevance of repulsive intermolecular interactions in the crystals of forms **II** and **III** compared with form **I**. Repulsions are much probably due mostly to methyl⋯methyl and (ring methylene)⋯(ring methylene) repulsions. In form **I**, only the first type of interactions exist (in a top-to-top arrangement), while in forms **II** and **III** both types of interaction exist. In

form **II**, both interactions are of stacking type, since the molecules of adjacent layers are nearly superposed to each other, while in form **III** methyl⋯methyl repulsive interactions are of stacking type (with molecules oriented in opposite directions) and (ring methylene)⋯(ring methylene) interactions are top-to-top.

### 3.3. Selection of the computational model

The computational study of the polymorphs of 1-MH started by the selection of the theoretical model. The chosen combinations of functional and basis sets were used to predict the unit cell parameters as a measure of the quality of the model. The empirical correction for dispersion interaction (DFT-D) proposed by Grimme<sup>28–30</sup> was also applied in order to consider van der Waals and other dispersion attractive interaction forces. The obtained results are presented in Table 3. The set of parameters for the Grimme correction are reported in Table S1.†

According to the data shown in Table 3, among the different models benchmarked, the B3LYP-D/6-31G(d,p) yields the results exhibiting the best agreement with the experimental data. This indicates that the hydrogen-bonding effects (the dominating effects in the studied crystals) are described accurately by this computational approach, and in particular that the use of the Grimme correction<sup>28–32</sup> considerably improves the theoretical predictions. These results are in agreement with data obtained previously for other systems,<sup>33–37</sup> and justify the use of the B3LYP-D/6-31G(d,p) model in the theoretical structural and spectroscopic analyses presented in sections 3.4, 3.5 and 3.6.

### 3.4. Computational structural results

The crystal structures of the three polymorphs of 1-MH were optimized using the selected theoretical model. These calculations allowed to estimate the relative energies of the crystals. Also, the comparison between the calculated and experimental geometries allowed an additional test to the quality of the theoretical model, which we wanted to apply to help interpretation of the spectroscopic data (both Raman and infrared) for the different forms of 1-MH.

The detailed structural results are provided in Tables S2–S4 (ESI†), and are summarized in Fig. 6 in a compact graphical format. In general terms, it can be concluded that the B3LYP-D/6-31G(d,p) model reproduces appropriately the experimental structural data, in line with what was already observed for the cell parameters. This result increased our confidence in the appropriateness of the theoretical model also for prediction of the vibrational spectra.

The relative energies obtained from the calculations indicate that the most stable crystallographic structure of 1-MH is the polymorph **I**, in agreement with the experimental data.<sup>7</sup> The new form **III** was predicted to have an energy higher than that of polymorph **I** by 2.42 kJ mol<sup>-1</sup>, while form **II** has a predicted energy 11.46 kJ mol<sup>-1</sup> higher than polymorph **I**. As mentioned above, the reasons for the relative

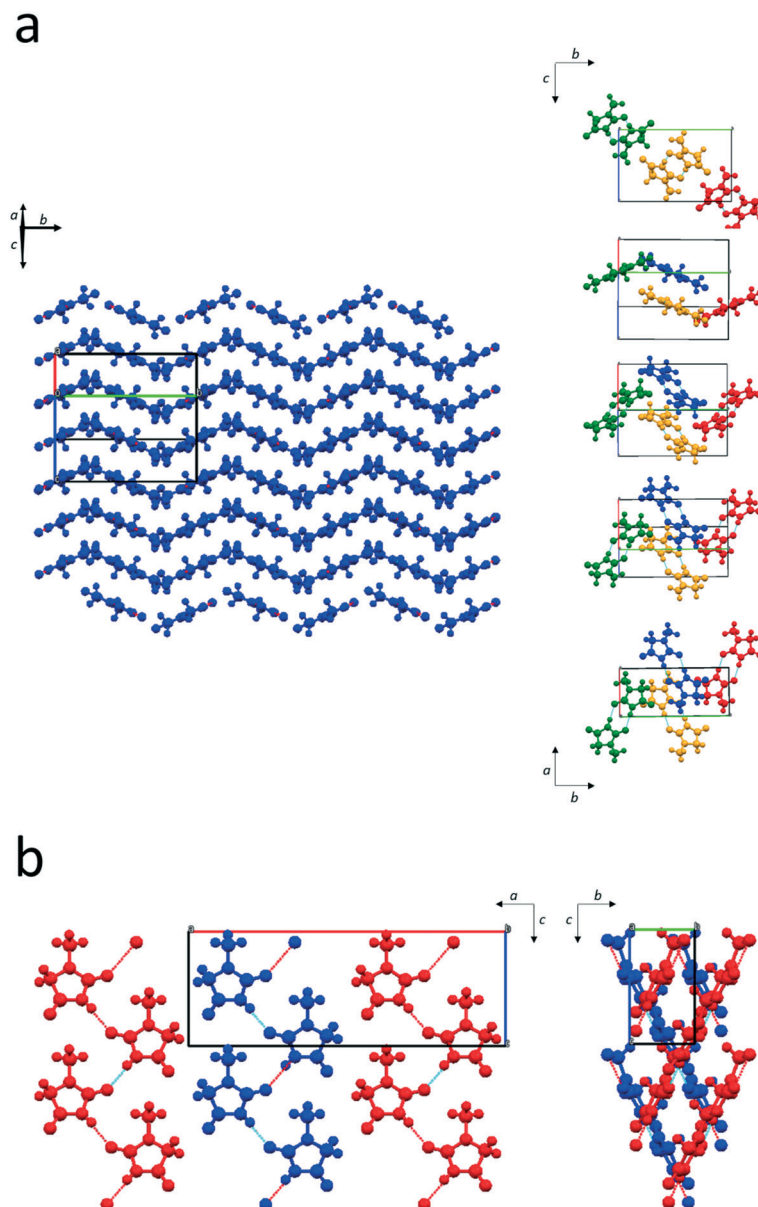


**Fig. 5** (a: top panel) Projection of the structure of polymorph I showing the chains built from dimeric units of 1-MH (left) and sequence of projections showing the dimeric units and how they relate spatially (right); this sequence of projections are related by rotation about the *b* axis; the colours are used to distinguish the dimers and do not mean that molecules are symmetry independent. (b: bottom) Projection of the structure of polymorph II viewed along the *b* axis (left) and along the *a* axis; the colours are used to highlight the two sets of interspersed chains, and do not mean that the molecules are symmetry independent.

energies of the crystals of the three 1-MH forms shall involve several factors (strength of hydrogen bonds, steric stress, staking interactions, conformational adjustments, *etc.*) which cannot be scrutinized individually in a quantitative way. However, as it was also already referred to before, the fact that the relative energies of the polymorphs correlate inversely with the densities points to a greater relevance of repulsive intermolecular interactions in the crystals of forms **II** and **III** than in form **I**.

Once the relative energies of the crystals have been determined, lattice energies for the different polymorphs of 1-MH could be computed using the CE-B3LYP model,<sup>38</sup> and

related with sublimation enthalpies  $\Delta H_{\text{sub}}(T)$ . According to the CE-B3LYP approach:

$$\begin{aligned}\Delta H_{\text{sub}}(T) &= (E_{\text{el}}^{\text{g}} + E_{\text{trans}}^{\text{g}} + E_{\text{rot}}^{\text{g}} + E_{\text{vib}}^{\text{g}}) - (E_{\text{el}}^{\text{s}} + E_{\text{vib}}^{\text{s}}) + pV \\ &= (E_{\text{el}}^{\text{g}} - E_{\text{el}}^{\text{s}}) + (E_{\text{vib}}^{\text{g}} - E_{\text{vib}}^{\text{s}}) + 4RT \\ &= \Delta E_{\text{el}} + \Delta E_{\text{vib}} + 4RT \\ &= -\Delta E_{\text{lat}} + \Delta E_{\text{vib}} + 4RT\end{aligned}\quad (1)$$

where ideal gas behavior is assumed, and the superscripts *g* and *s* refer to the gas and solid crystalline states. Several approaches have been used to obtain “experimental” benchmark lattice energies by estimating the thermal effects,

**Table 3** Comparison between the experimental and the computed unit cell parameters of 1-MH polymorphs<sup>a</sup>

		B3LYP				B3LYP-D				PBE0-D	
Exp.		pob-TZVP	% <i>E</i>	6-31G(d,p)	% <i>E</i>	pob-TZVP	% <i>E</i>	6-31G(d,p)	% <i>E</i>	6-31G(d,p)	% <i>E</i>
Polymorph I monoclinic ( <i>Z</i> = 4) <i>P</i> 2 <sub>1</sub> / <i>c</i>											
<i>a</i>	5.601	5.841	4.3	5.864	4.7	5.502	−1.8	5.465	−2.4	5.373	−4.1
<i>b</i>	12.178	12.436	2.1	12.266	0.7	12.174	0.0	12.055	−1.0	11.979	−1.6
<i>B</i>	8.090	8.226	1.7	8.204	1.4	7.756	−4.1	7.859	−2.9	7.715	−4.6
<i>β</i>	105.64	107.15	1.4	107.46	1.7	103.20	−2.3	103.22	−2.3	102.38	−3.1
Volume	531.4	570.9	7.4	563.0	5.9	505.8	−4.8	504.0	−5.2	485.0	−8.7
Polymorph II orthorhombic ( <i>Z</i> = 4) <i>Pna</i> 2 <sub>1</sub>											
<i>a</i>	19.026	19.126	0.5	19.154	0.7	18.716	−1.6	18.734	−1.5	18.553	−2.5
<i>b</i>	3.912	4.129	5.5	4.149	6.1	3.811	−2.6	3.821	−2.3	3.745	−4.3
<i>c</i>	6.829	6.850	0.3	6.817	−0.2	6.821	−0.1	6.804	−0.4	6.773	−0.8
Volume	508.3	540.9	6.4	541.8	6.6	486.6	−4.3	487.1	−4.2	470.6	−7.4
Polymorph III orthorhombic ( <i>Z</i> = 12) <i>P</i> 2 <sub>1</sub> 2 <sub>1</sub> 2 <sub>1</sub>											
<i>a</i>	7.847	7.860	0.2	7.825	−0.3	7.842	−0.1	7.815	−0.4	7.780	−0.9
<i>b</i>	9.826	9.892	0.7	9.868	0.4	9.702	−1.3	9.749	−0.8	9.644	−1.8
<i>c</i>	20.311	22.249	9.5	21.748	7.1	19.530	−3.8	19.509	−3.9	19.114	−5.9
Volume	1565.9	1729.6	10.5	1679.4	7.2	1485.9	−5.1	1486.4	−5.1	1434.1	−8.4

<sup>a</sup> Values of *a*, *b* and *c* are in Å,  $\beta$  in degrees, and volume in Å<sup>3</sup>. B3LYP-D refers to DFT calculation where the Grimme correction for dispersion interaction (DFT-D) was used. For each cell parameter, the percentage error (% E) with respect to the experimental data was calculated as % E = ((PAR<sub>theo</sub> - PAR<sub>exp</sub>)/PAR<sub>exp</sub>) × 100, where PAR refers to the cell parameter (*a*, *b*, *c*,  $\beta$  or volume).

$\Delta E_{\text{vib}} + 4RT$ , at different levels of sophistication. The most common approximates these two terms by  $-2RT$ , a result that assumes no difference between gas and crystal intramolecular vibrations, and the intermolecular vibrational energy is at the high-temperature limit of  $6RT$ . These and other assumptions underlying this approximation are discussed in detail in several places.<sup>39–43</sup>

Since

$$-E_{\text{lat}} = \Delta E_{\text{el}} = (E_{\text{el}}^{\text{g}} - E_{\text{el}}^{\text{s}}) \quad (2)$$

and in 1-methylhydantoin, which is a conformationally rigid molecule,  $E_{\text{el}}^{\text{g}}$  is constant, knowing  $E_{\text{lat}}$  for one polymorph allows to derive the lattice energy for the remaining polymorphs, once known the corresponding  $E_{\text{el}}^{\text{s}}$  values calculated using full periodic conditions. Under these assumptions, the differences in the calculated lattice energies of the polymorphs are equal to the differences between their electronic energies.

The lattice energy for polymorph **I** was then calculated using the CE-B3LYP model (with the 6-31G(d,p) basis set and the CrystalExplorer17 software),<sup>44</sup> and then eqn (1) and (2) were used to obtain the lattice energies for the remaining polymorphs as well as the sublimation enthalpies at room temperature for all polymorphic forms. In the CE-B3LYP calculations molecules within a radius of 20 Å were considered. The CE-B3LYP calculated lattice energy for form **I** is  $-111 \text{ kJ mol}^{-1}$ , and those obtained for forms **II** and **III**,  $-100$  and  $-109 \text{ kJ mol}^{-1}$ , respectively. Estimated sublimation energies are 106, 95 and  $104 \text{ kJ mol}^{-1}$ , for forms **I**, **II** and **III**, respectively.

In the plots shown in Fig. 6, we can clearly see that the calculated 1-MH molecular geometries for all three polymorphs reproduce very well the experimental ones. This

is not an unexpected result, since the used model was selected based on its good performance in predicting the more difficult to fit unit cell parameters, as described in the previous section. Moreover, 1-MH is a rather rigid molecule, which is also a factor contributing to the observed good reproduction of the experimental data by the calculations. For polymorph **I**, the largest difference between the experimental and calculated bond lengths amounts to only 0.02 Å for N1–C2 and C4–C5 bonds, while the largest differences for the bond and torsion angles are 0.3° (C5–N1–C6) and 3.1° (C6–N1–C5–C4), respectively. Similar values were found for the other forms: for polymorph **II**, the largest differences in the bond lengths, bond angles and torsion angles are 0.02 Å (N1–C2, N1–C5, C4=O9 and C4–C5), 1.3° (C5–N1–C6), and 1.2° (C6–N1–C2=O7), respectively, whereas for polymorph **III**, these values are respectively 0.02 Å (several bonds in all three symmetry non-equivalent molecules of the crystal), 0.9° (C2–N1–C6 of molecule A), and 3.0° (C2–N3–C4–C5 and N3–C4–C5–N1 of molecule A). The total r.m.s. errors for all bond lengths, and bond and torsion angles not-involving hydrogen atoms of the polymorphs are (0.013 Å, 0.15°, 1.68°), (0.015 Å, 0.56°, 0.70°) and (0.015 Å, 0.40°, 1.28°), for forms **I**, **II** and **III**, respectively.

### 3.5. IR spectroscopy of 1-MH polymorphs

Fig. 7 shows the room temperature experimental IR spectra of polymorphs **I** and **II** taken from our previous work,<sup>6</sup> and the B3LYP-D/6-31G(d,p) calculated spectra for the three forms. Unfortunately the experimental IR spectrum of polymorph **III** could not be registered because of the small amount of this material obtained. The experimental spectra were recorded in the attenuated total reflectance (ATR) mode, so that the spectra here presented have been subjected to

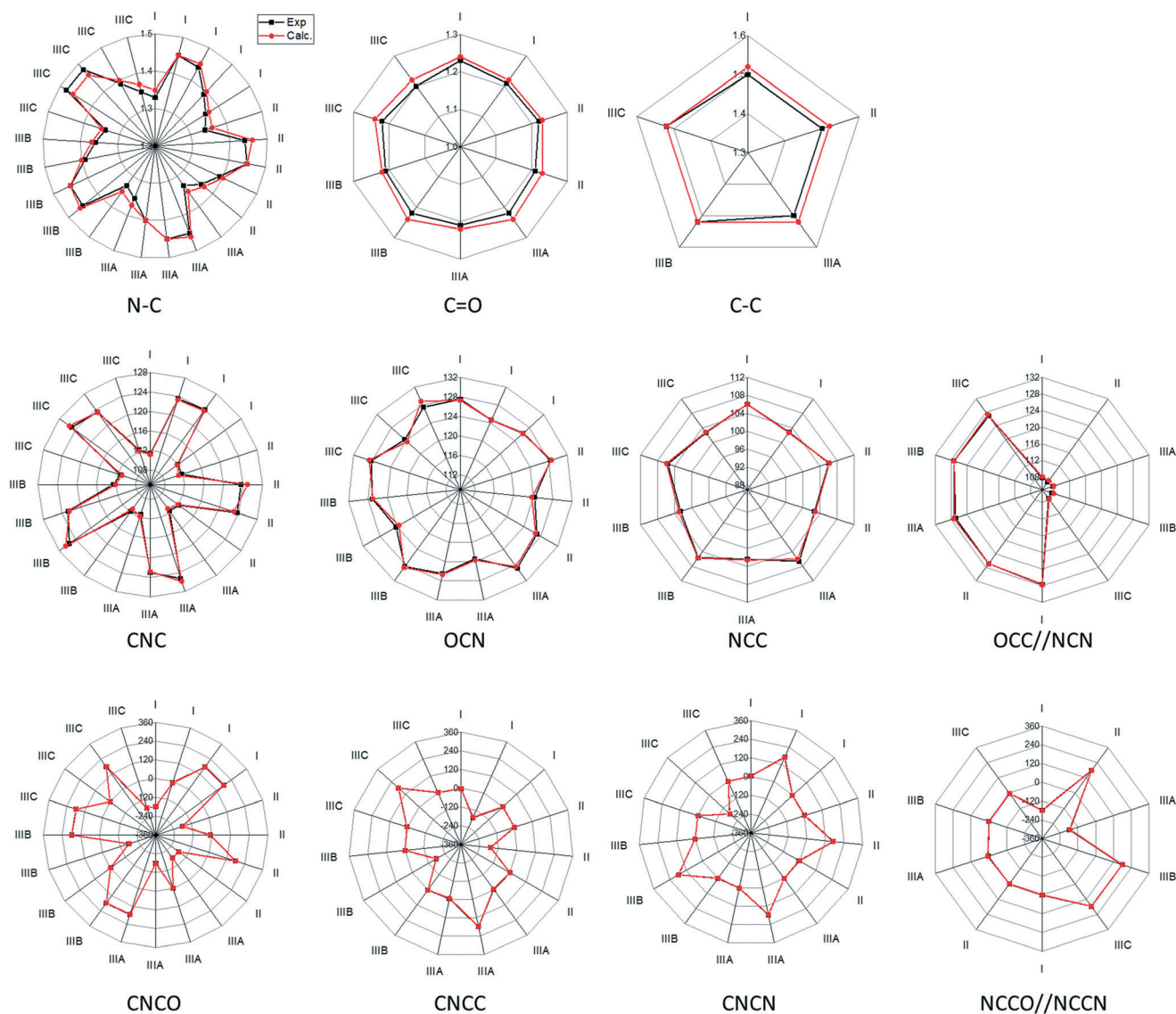


**Fig. 6** Radar type plots showing the values of the experimental (black squares) and B3LYP-D/6-31G(d,p) calculated (red circles) bond lengths (Å), bond angles (°) and torsion angles (°) for the three polymorphs of 1-MH. For polymorph III, values for the three non-equivalent by symmetry molecules are included. For each type of coordinate, scales were chosen to allow direct comparison between the various plots.

ATR correction<sup>45</sup> before comparison with the calculated absorption spectra.

The data is shown in Fig. 7 in different ways, to allow for easier comparison between the experimental spectra of the polymorphs and also between these spectra and the calculated ones. As it can be seen in the figure, the agreement between the experimental and the calculated IR spectra is very good, both regarding frequencies and relative intensities, which demonstrate the reliability of the used computational method in predicting these properties. Table 4 presents the experimental and calculated frequencies for forms **I** and **II** and the predicted IR frequencies for form **III** and their respective assignments based on the normal modes description resulting from the fully periodic B3LYP-D/6-31G(d,p) vibrational calculations.

Based on the comparative analysis of the spectra of the different polymorphs, we have chosen characteristic marker-bands for each material, for their fast identification. These marker-bands are highlighted in Fig. 7 and Table 4 by the symbols o, + and x, for forms **I**, **II** and **III**, respectively. These bands are due to the  $\nu(\text{C}=\text{O})$  and  $\gamma(\text{NH})$  vibrational modes and the corresponding spectral regions are represented in Fig. 7 in an expanded way for better visualization. The first marker-band is an intense band (with minor associated satellite bands) observed at  $1690\text{ cm}^{-1}$  and  $1729\text{ cm}^{-1}$  for polymorphs **I** and **II**, respectively (predicted values:  $1685\text{ cm}^{-1}$  and  $1715\text{ cm}^{-1}$ ). For polymorph **III**, this band is predicted at  $1700\text{ cm}^{-1}$  and can be expected to be observed at *ca.*  $1709\text{ cm}^{-1}$  if the shift from the corresponding calculated value is similar to those observed for the remaining two forms. The second marker-band is observed experimentally at

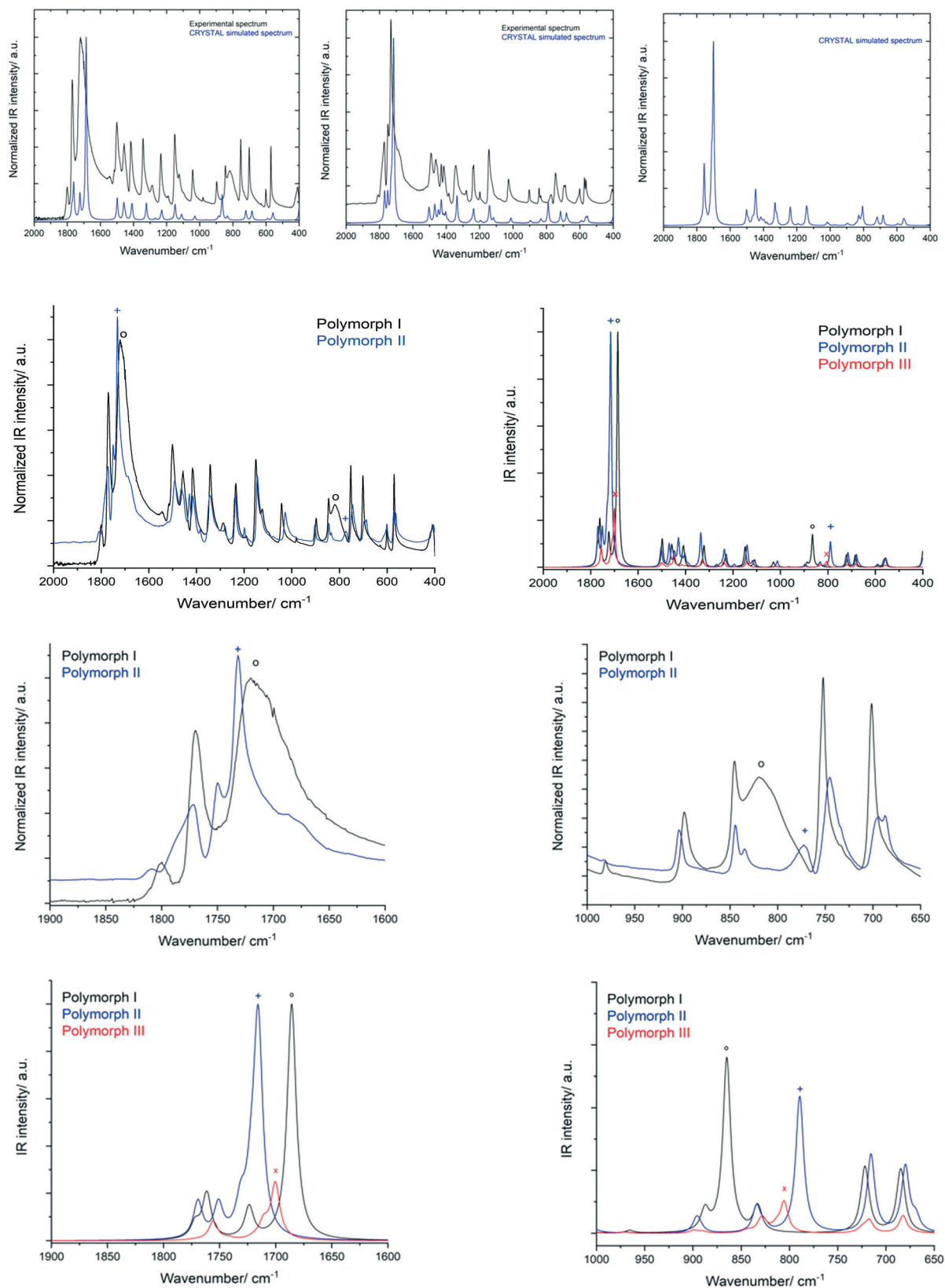


**Fig. 7** First row: comparison of the experimental and B3LYP-D/6-31G(d,p) calculated IR spectra of polymorph I (left panel), polymorph II (center) and polymorph III (right). Second row: comparison of the experimental IR spectra of the polymorphs (left panel) and of the calculated spectra (right). Third and fourth rows: expansions of selected spectral IR regions allowing comparison of the experimental spectra to each other and between these spectra and the calculated ones. Marker bands of I, II and III are indicated by o, + and x respectively (see text).

**Table 4** Observed IR bands of polymorphs I and II of 1-MH and B3LYP-D/6-31G(d,p) calculated frequencies for the three polymorphs, with proposed assignments<sup>a</sup>

Calc. Monomer	Exp.	Calc. Polymorph I	Exp.	Calc. Polymorph II	Calc. Polymorph III	Assignment <sup>b</sup>
3534	3136/ <b>3030</b>	<b>3102</b> /3097	<b>3128</b> /3072	<b>3179</b> /3147	<b>3239</b> /3221	$\nu(\text{NH})$
					<b>3197</b> / <b>3185</b>	
3050	2986	3089	2988	3084	3076	$\nu(\text{CH}_3)_{\text{as}}'$
2971	2956	3048	2955	3049	3037	$\nu(\text{CH}_3)_{\text{as}}''$
2958	2956	3026	2939	3023	3032	$\nu(\text{CH}_2)_{\text{as}}$
2926	2928	2980	2928	2987	2973	$\nu(\text{CH}_2)_{\text{s}}$
2920	2887	2961	2886	2978	2968	$\nu(\text{CH}_3)_{\text{s}}$
1813	1800/ <b>1767</b>	1772/ <b>1762</b>	<b>1771</b> /1749	<b>1768</b> /1750	<b>1756</b> /1743	$\nu(\text{C=O})$
1783	1718/ <b>1690</b>	1724/ <b>1685</b>	o <b>1729</b> /1716	1730/ <b>1715</b>	+ 1710/ <b>1700</b>	x $\nu(\text{C=O})$
1487	1516	1498	1519	1503	1501	$\delta(\text{CH}_3)_{\text{as}}'$
1310	1497	1412	1489	1415	1380	$\delta(\text{NH})$
1451	1455	1458	1462	1469	1467	$\delta(\text{CH}_3)_{\text{as}}''$
1450	1455	1453	1455	1447	1447	$\delta(\text{CH}_2)$
1410	1421	1421	1429	1430	1416	$\delta(\text{CH}_3)_{\text{s}}$
1394	1417/ <b>1412</b>	1411/1407	1414	1403	1398	$\nu_2(\text{ring})$
1288	1340	1322	1341	1336	<b>1331</b> /1322	$\nu_4(\text{ring})^c$
1271	1286	1270	1280	1256	1240	$\nu(\text{NC})$
1215	1233	1229	1240/1235	1246/1236	1236	w( $\text{CH}_2$ )
1158	1199/ <b>1190</b>	<b>1177</b> /1166	1199	1195	1192	tw( $\text{CH}_2$ )
1093	<b>1148</b> /1145	1152/ <b>1149</b>	1143	1141	1141	$\nu_1(\text{ring})^c$
n.obs.	<b>1123</b> /1099	1113/ <b>1110</b>	1126	1118	1114	$\gamma(\text{CH}_3)''$
n.obs.	1042	1029	n.obs.	n.obs.	970	$\gamma(\text{CH}_2)$
1013	981	965	1026	1013	<b>1019</b> /1012	$\gamma(\text{CH}_3)'$
859	897	887	903	896	<b>899</b> /892	$\nu_5(\text{ring})$
794	844	834	835	833	828	$\nu_3(\text{ring})$
573	807	865	o 772	789	+ 842/828/ <b>806</b>	x $\gamma(\text{NH})$
718	751	722	744	716	718	$\gamma(\text{C=O})$
669	699	685	687	680	682	$\delta_1(\text{ring})$
569	601	590	601	590	595	$\delta_2(\text{ring})$
535	569	560	571	564	560	$\delta(\text{C=O})$
522	569	555	563	555	549	$\gamma(\text{C=O})$

<sup>a</sup> Frequencies in  $\text{cm}^{-1}$  (predicted frequencies scaled by 0.9648). Bold numbers represent the most intense band when there are more than one band assigned to one vibration. Mark bands for the polymorphs are indicated by the symbols o, + and x, respectively for polymorphs I, II and III (see text). <sup>b</sup> See Fig. 1 for atom numbering. Assignments correspond to approximate descriptions of the vibrations chosen as the main coordinate contributing to the vibration (avoiding repetition) and are based on the normal modes description resulting from the fully periodic vibrational calculations. Abbreviations: w, wagging; tw, twisting;  $\gamma$ , rocking;  $\nu$ , stretching;  $\delta$ , bending;  $\tau$ , torsion; s, symmetric; as, anti-symmetric; n.obs., not observed. <sup>c</sup> Also with a significant contribution from the  $\delta(\text{NH})$  coordinate.

807  $\text{cm}^{-1}$  and 772  $\text{cm}^{-1}$  for polymorphs I and II, respectively, and calculated at 865  $\text{cm}^{-1}$  and 789  $\text{cm}^{-1}$ . The calculated frequency is 806  $\text{cm}^{-1}$  for the case of polymorph III, which indicates that the experimental band for this form can be expected to be observed approximately at the mid frequency between the bands of polymorphs I and II.

It is interesting to note that, not surprisingly, the chosen marker-bands correspond to vibrations ( $\nu(\text{C=O})$  and  $\gamma(\text{NH})$  vibrations) which are localized in the moieties that directly participate in the hydrogen-bonding network of the crystals. It is also worth mentioning that these bands are also the broadest bands in the spectra, which is also a direct consequence of hydrogen bonding. The bands of polymorph I are, in this respect, particularly noticeable, what is in

agreement with the existence of stronger hydrogen bonds in the crystal of this form.

### 3.6. Raman spectroscopy of 1-MH polymorphs

The Raman spectra of the three 1-MH polymorphs are displayed in Fig. 8, where they may be compared to each others and also with the B3LYP-D/6-31G(d,p) calculated spectra. As for the infrared spectra, the calculated Raman spectra show a general good agreement with the experimental ones, in particular regarding frequencies. Assignments are presented in Table 5.

Also, as it was done in the case of the infrared spectra, we elected a few marker-bands for quick identification of the

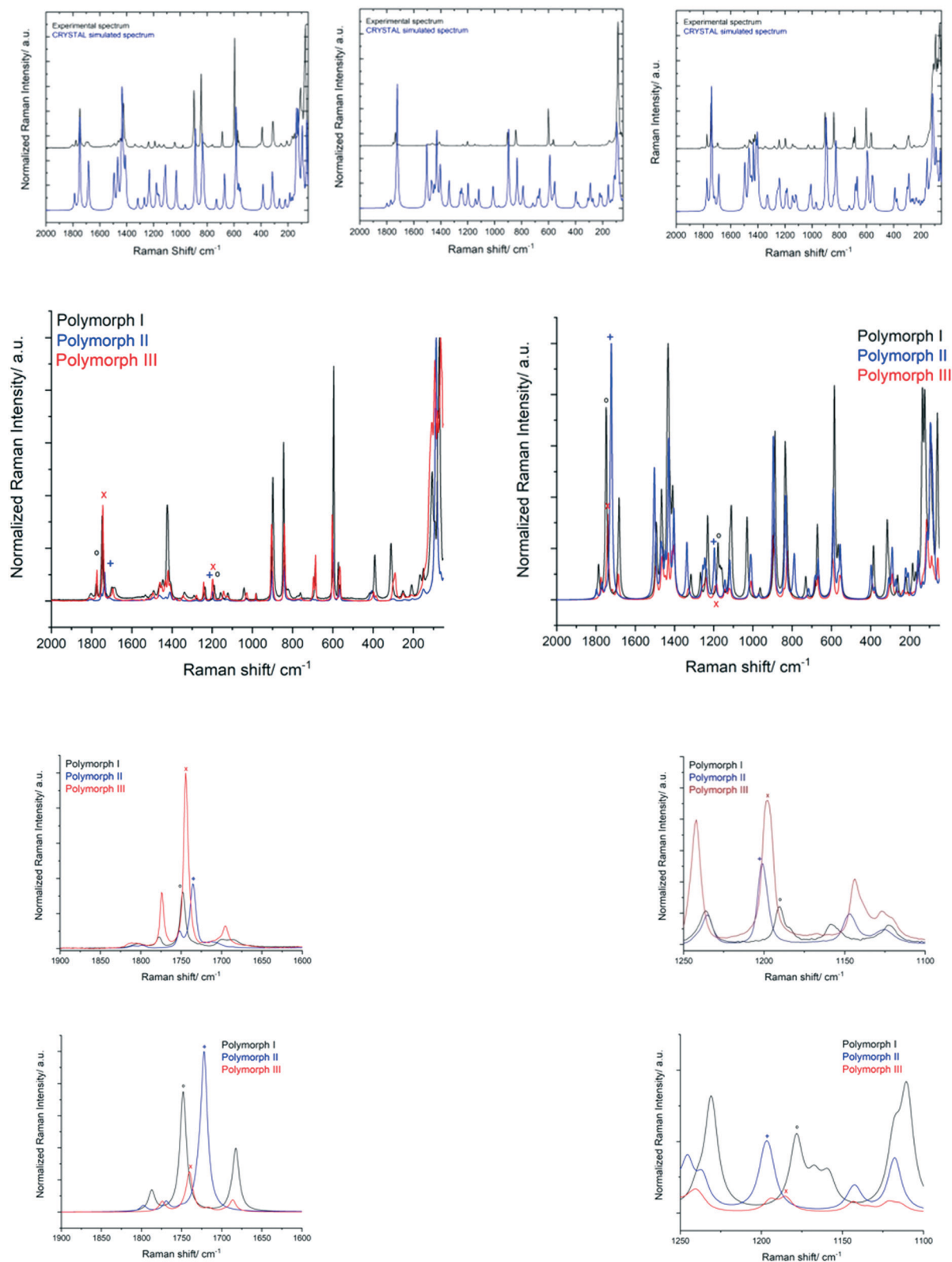


**Fig. 8** First row: comparison of the experimental and B3LYP-D/6-31G(d,p) calculated Raman spectra of polymorph I (left panel), polymorph II (center) and polymorph III (right). Second row: comparison of the experimental IR spectra of the polymorphs (left panel) and of the calculated spectra (right). Third and fourth rows: expansions of selected spectral IR regions allowing comparison of the experimental spectra to each other and between these spectra and the calculated ones. Marker bands of I, II and III are indicated by o, + and x respectively (see text).

**Table 5** Observed Raman bands of polymorphs I, II and III of 1-MH and B3LYP-D/6-31G(d,p) calculated frequencies, with proposed assignments<sup>a</sup>

Calc. Monomer 3534	Exp. Polymorph I 3014	Calc. 3069	Exp. Polymorph II 3131	Calc. 3208 3179 <b>3147</b>	Exp. Polymorph III 3170	Calc. 3241 3239 3221 3198 3186 <b>3184</b> <b>3075</b> 3070 3046 <b>3044</b> 3038 3031 <b>2982</b> 2973	Assignment <sup>b</sup> ν(NH)
3050	2981	3088	3074	3085	3068	3075	ν(CH <sub>3</sub> ) <sub>as</sub> '
2971	2957	3049	3023	3049	3013	3046	ν(CH <sub>3</sub> ) <sub>as</sub> "
2958	2957	3026	2983	3023	2956	3038	ν(CH <sub>2</sub> ) <sub>as</sub>
2926	2929	2981	2953	2987	2936	3031	ν(CH <sub>2</sub> ) <sub>s</sub>
2921	2883	2966	2940	2979	2886	<b>2982</b> 2973	ν(CH <sub>3</sub> ) <sub>s</sub>
1813	1777 <b>1748 o</b>	1787 <b>1749</b>	1752 <b>1735 +</b>	1751 <b>1722</b>	1774 <b>1744 x</b>	1777 1775 1772 1745 1743 <b>1741</b>	ν(C=O9)
1783	1698 <b>1686</b>	1690 <b>1683</b>	1809 1798 <b>1714</b>	1798 <b>1769</b> 1728	1720 <b>1695</b>	1720 1717 1712 1696 1691 1689 <b>1687</b> <b>1496</b> 1492	ν(C=O7)
1487	1491	1495 <b>1491</b>	1520	1507 <b>1504</b> 1501	1495	1496 1492	δ(CH <sub>3</sub> ) <sub>as</sub> '
1310	1423	1430	1492	1406 <b>1403</b> 1389	1380	1386 <b>1383</b> 1365	δ(NH)
1451	1463	<b>1467</b> 1460	1463	<b>1470</b> 1462	1460	1468 1465 <b>1462</b>	δ(CH <sub>3</sub> ) <sub>as</sub> "
1450	1423	<b>1425</b> 1420	1454	1468	1450	1451 <b>1447</b>	δ(CH <sub>2</sub> )
1410	1445	1435	1430	1447	1432	1433	δ(CH <sub>3</sub> ) <sub>s</sub>
1394	1406	<b>1409</b> 1403	1411	1430	1430	1414 1411 <b>1412</b>	ν <sub>2</sub> (ring)
1288	1338	1316	1353	1337	1345	1333 <b>1329</b> 1324	ν <sub>4</sub> (ring) <sup>b</sup>
1271	1290	1269	1280	1256	1278	1259 <b>1255</b>	ν(NC)
1215	1236	1239 <b>1231</b>	1235	<b>1246</b> 1237	1242	1243 <b>1239</b>	w(CH <sub>2</sub> )
1158	1190 o	<b>1178</b> 1167	1201 +	<b>1199</b> 1195	1198 x	1193 <b>1186</b>	tw(CH <sub>2</sub> )
1113	1123	1118 <b>1110</b>	1125	1118	1127	<b>1121</b> 1117 1114	γ(CH <sub>3</sub> )"
1093	1159	1158	1147	1142	1144	1144	ν <sub>1</sub> (ring) <sup>b</sup>
1013	1042	1034 <b>1030</b>	1030	<b>1014</b> 1009	1028	1021 <b>1011</b> 1008	γ(CH <sub>3</sub> )'
980	981	965	983	971	983	<b>972</b> 969	γ(CH <sub>2</sub> )
859	898	892 <b>888</b>	904	900 <b>897</b> 893	905	<b>899</b> 895 891	ν <sub>2</sub> (ring)
794	845	835	844	<b>834</b> 824	777	<b>826</b> 811	ν <sub>3</sub> (ring)
573	823	828	770	798 793 <b>790</b>	840	844 <b>841</b>	γ(NH)
718	761	731	746	718	763	<b>728</b> 724	γ(C=O7)
669	688	672	687	685 680 <b>668</b> <b>590</b>	697 <b>687</b> <b>670</b>	683 <b>670</b>	δ <sub>1</sub> (ring)
569	596	585	601	593 <b>590</b>	603	595	δ <sub>2</sub> (ring)
535	573	567	574	565	568	558	δ(C=O7)
522	566	<b>554</b> 548	565	555	565	550	γ(C=O9)
369	392	386	406	402 <b>398</b>	<b>397</b> 385	<b>391</b> 376	δ(C=O9)
276	311	<b>315</b> 307	304	308 296 <b>290</b>	299 <b>291</b>	305 300 295 <b>289</b> 269	δ(NC)
191	253	263	241	271	250	255 243 <b>234</b> 225 215 <b>212</b>	τ <sub>1</sub> (ring)
162	208	<b>221</b> 218	205	<b>221/209</b>	209	225 215 <b>212</b>	τ <sub>2</sub> (ring)

<sup>a</sup> Frequencies in cm<sup>-1</sup> (predicted frequencies scaled by 0.9648). Bold numbers represent the most intense band when there are more than one band assigned to one vibration. Mark bands for the polymorphs are indicated by the symbols o, + and x, respectively for polymorphs I, II and III (see text). <sup>b</sup> See Fig. 1 for atom numbering. Assignments correspond to approximate descriptions of the vibrations chosen as the main coordinate contributing to the vibration (avoiding repetition) are based on the normal modes description resulting from the fully periodic vibrational calculations. Abbreviations: w, wagging; tw, twisting; γ, rocking; ν, stretching; δ, bending; τ, torsion; s, symmetric; as, anti-symmetric; n.obs., not observed.

polymorphs. These marker-bands are associated with the  $\nu(\text{C}=\text{O})$  and the  $\text{tw}(\text{CH}_2)$  vibrations. The corresponding spectral ranges are depicted in an expanded scale in Fig. 8. They are identified in this figure and also in Table 5 by the symbols o, + and x, for forms **I**, **II** and **III**, respectively.

The first set of marker-bands appears at 1748, 1735 and 1744  $\text{cm}^{-1}$  for polymorphs **I**, **II** and **III**, respectively, the corresponding calculated frequencies being 1749, 1722 and 1744  $\text{cm}^{-1}$ . The second set of marker-bands comprehends the bands observed at 1190  $\text{cm}^{-1}$  (form **I**), 1201  $\text{cm}^{-1}$  (form **II**) and 1198  $\text{cm}^{-1}$  (form **III**), whose corresponding calculated frequency values are 1178, 1199 and 1186  $\text{cm}^{-1}$ , respectively.

## 4. Conclusions

In this study, a new polymorph (form **III**) of 1-MH was described. The new polymorph crystallizes in the orthorhombic Sohncke space group  $P2_12_12_1$  with cell parameters  $a = 7.8466(2)$ ,  $b = 9.8257(3)$ ,  $c = 20.3107(7)$  Å. Very interestingly, the crystal of form **III** was found to exhibit a high- $Z'$  ( $Z' = 3$ ) asymmetric unit and 12 molecules in the unit cell ( $Z = 12$ ), which contrasts with the simpler crystal structures found previously for polymorphs **I** and **II** ( $Z = 4$ ;  $Z' = 1$ ).<sup>7,18</sup> The new crystalline variety was predicted by the DFT-D/6-31G(d,p) fully periodic calculations to be higher in energy than form **I** (in consonance with the experimental data),<sup>7</sup> but lower in energy than form **II**.

The comparison between the structures of the crystals of the three polymorphs of 1-MH allowed identifying similarities and dissimilarities between the three forms. Polymorphs **II** and **III** share the common fact of having the molecules of 1-MH linked by  $\text{N3-H}\cdots\text{O7}$  and forming chains, while in polymorph **I** the molecules form dimers (also through  $\text{N3-H}\cdots\text{O7}$  H-bond interactions) which then associate in chains. Nevertheless, the way the chains of molecules in the crystals of polymorphs **II** and **III** are packed in a very different way. In form **III** they pack in parallel layers forming an A, B + C, B + C, A pattern, where A, B and C are the three symmetry independent molecules in the unit cell, while in form **II** the chains are interspersed with each other forming an angle of ca. 36°.

The densities of the three polymorphs was found to follow the order **I** < **III** < **II**, which is the same order as the relative energies of the corresponding crystals predicted by the DFT calculations. The fact that the relative energies of the crystal correlate inversely with the densities point to the relevance of repulsive intermolecular interactions in the crystals of polymorphs **II** and **III** compared with polymorph **I**.

The experimental IR and Raman spectra of the polymorphs were also investigated (or revisited, in the case of forms **I** and **II**), with help of the fully periodic DFT-D/6-31G(d,p) calculations, and assigned in detail. Marker-bands in the infrared and Raman spectra of the polymorphs were proposed for their fast spectroscopic identification.

## Conflicts of interest

There are no conflicts to declare.

## Acknowledgements

The authors acknowledge financial support from the Portuguese Science Foundation ("Fundação para a Ciência e a Tecnologia" – FCT) – Projects CQC UIDB/00313/2020 and UIDP/00313/2020, also co-funded by FEDER/COMPETE 2020-EU. CFisUC is funded by FCT through the projects UIDB/04564/2020 and UIDP/04564/2020. Access to instruments from Laser-Lab Coimbra and TAIL-UC facilities funded under QREN-Mais Centro is gratefully acknowledged. B. A. N. also acknowledges FCT for the SFRH/BD/129852/2017 PhD Scholarship.

## References

- 1 J. Bernstein, *Polymorphism in Molecular Crystals*, Oxford University Press, 2010.
- 2 J. Bernstein, *Cryst. Growth Des.*, 2011, **11**, 632.
- 3 R. Fausto, G. O. Ildiz, E. M. Brás and B. A. Nogueira, Hydantoins and Mercaptoimidazoles: Vibrational Spectroscopy as a Probe of Structure and Reactivity in Different Environments, from the Isolated Molecule to Polymorphs, in *Challenges and Advances in Computational Chemistry and Physics*, ed. J. Leszczynski, Springer Nature, 2019, vol. 26, p. 199.
- 4 G. O. Ildiz, I. Boz and O. Unsalan, *Opt. Spectrosc.*, 2012, **112**, 665.
- 5 G. O. Ildiz, C. M. Nunes and R. Fausto, *J. Phys. Chem. A*, 2013, **117**, 726.
- 6 B. A. Nogueira, G. O. Ildiz, J. Canotilho, M. E. S. Eusébio and R. Fausto, *J. Phys. Chem. A*, 2014, **118**, 5994.
- 7 B. A. Nogueira, G. O. Ildiz, M. S. C. Henriques, J. A. Paixão and R. Fausto, *J. Mol. Struct.*, 2017, **1148**, 111.
- 8 B. A. Nogueira, G. O. Ildiz, J. Canotilho, M. E. S. Eusébio, M. S. C. Henriques, J. A. Paixão and R. Fausto, *J. Phys. Chem. A*, 2017, **121**, 5267.
- 9 B. A. Nogueira, G. O. Ildiz, J. Canotilho, M. E. S. Eusébio, J. A. Paixão and R. Fausto, *J. Phys. Chem. A*, 2020, **124**, 6303.
- 10 B. A. Nogueira, G. O. Ildiz, A. M. Tabanez, M. S. C. Henriques, J. A. Paixão and R. Fausto, *J. Mol. Struct.*, 2020, **1222**, 128897.
- 11 S. S. Block, *Disinfection, Sterilization, and Preservation*, Lippincott Williams & Wilkins, 2001.
- 12 C. S. A. Kumar, C. V. Kavitha, K. Vinaya, S. B. B. Prasad, N. R. Thimmegowda, S. Chandrappa, S. C. Raghavan and K. S. Rangappa, *Invest. New Drugs*, 2009, **27**, 327.
- 13 C. V. Kavitha, M. Nambiar, C. S. A. Kumar, B. Choudhary, K. Muniyappa, K. S. Rangappa and S. C. Raghavan, *Biochem. Pharmacol.*, 2009, **77**, 348.
- 14 R. Sarges, R. C. Schnur, M. J. Peterson and J. L. Belletire, *J. Med. Chem.*, 1988, **31**, 230.
- 15 K. Yang, Y. Tang and K. A. Iczkowski, *Am. J. Transl. Res.*, 2010, **2**, 88.

- 16 H. S. Park, H. J. Choi, H. S. Shin, K. L. Sang and M. S. Park, *Bull. Korean Chem. Soc.*, 2007, **28**, 751.
- 17 R. N. Comber, R. C. Reynolds, J. D. Friedrich, R. A. Manguikian, R. W. Buckheit, J. W. Truss, W. M. Shannon and J. A. Secrist, *J. Med. Chem.*, 1992, **35**, 3567.
- 18 M. Puszyńska-Tuszkano, M. Daszkiewicz, G. Maciejewska, Z. Staszak, J. Wietrzyk, B. Filip and M. Cieślak-Golonka, *Polyhedron*, 2011, **30**, 2016.
- 19 Bruker APEX2, SADABS, XPRED and SAINT-Plus, Bruker AXS Inc., Madison, USA, 2004.
- 20 G. M. Sheldrick, *Acta Crystallogr., Sect. A: Found. Adv.*, 2015, **71**, 3.
- 21 G. M. Sheldrick, *Acta Crystallogr., Sect. C: Struct. Chem.*, 2015, **71**, 3.
- 22 R. Dovesi, A. Erba, R. Orlando, C. M. Zicovich-Wilson, B. Civalleri, L. Maschio, M. Rerat, S. Casassa, J. Baima, S. Salustro and B. Kirtman, *WIREs Comput. Mol. Sci.*, 2018, **8**, E1360.
- 23 R. Dovesi, V. R. Saunders, C. Roetti, R. Orlando, C. M. Zicovich-Wilson, F. Pascale, B. Civalleri, K. Doll, N. M. Harrison, I. J. Bush, P. D'Arco, M. Llunell, M. Causà, Y. Noël, L. Maschio, A. Erba, M. Rerat and S. Casassa, *CRYSTAL17 Users' Manual*, University of Turin, 2018.
- 24 A. D. Becke, *J. Chem. Phys.*, 1993, **98**, 5648.
- 25 C. Lee, W. Yang and R. G. Parr, *Phys. Rev. B: Condens. Matter Mater. Phys.*, 1988, **37**, 785.
- 26 C. Adamo and V. Barone, *J. Chem. Phys.*, 1999, **110**, 6158.
- 27 M. F. Peintinger, D. V. Oliveira and T. Bredow, *J. Comput. Chem.*, 2013, **34**, 451.
- 28 S. Grimme, *J. Comput. Chem.*, 2004, **25**, 1463.
- 29 S. Grimme, *J. Comput. Chem.*, 2006, **27**, 1787.
- 30 B. Civalleri, C. M. Zicovich-Wilson, L. Valenzano and P. Ugliengo, *CrystEngComm*, 2008, **10**, 405.
- 31 A. Bondi, *J. Phys. Chem.*, 1964, **68**, 441.
- 32 R. S. Rowland and R. Taylor, *J. Phys. Chem.*, 1996, **100**, 7384.
- 33 A. Milani and D. Galimberti, *Macromolecules*, 2014, **47**, 1046.
- 34 D. Galimberti and A. Milani, *J. Phys. Chem. B*, 2014, **118**, 1954.
- 35 C. Quarti, A. Milani and C. Castiglioni, *J. Phys. Chem. B*, 2013, **117**, 706.
- 36 D. Galimberti, C. Quarti, A. Milani, L. Brambilla, B. Civalleri and C. Castiglioni, *Vib. Spectrosc.*, 2013, **66**, 83.
- 37 C. Quarti, A. Milani, B. Civalleri, R. Orlando and C. Castiglioni, *J. Phys. Chem. B*, 2012, **116**, 8299.
- 38 S. P. Thomas, P. R. Spackman, D. Jayatilaka and M. A. Spackman, *J. Chem. Theory Comput.*, 2018, **14**, 1614.
- 39 A. Otero de la Roza and E. J. Johnson, *J. Chem. Phys.*, 2012, **137**, 054103.
- 40 A. M. Reilly and A. Tkatchenko, *J. Chem. Phys.*, 2013, **139**, 024705.
- 41 M. Cutini, B. Civalleri, M. Corno, R. Orlando, J. C. Brandenburg, L. Maschio and P. Ugliengo, *J. Chem. Theory Comput.*, 2016, **12**, 3340.
- 42 A. Gavezzotti and G. Filippini, in *Theoretical Aspects and Computer Modeling of the Molecular Solid State*, ed. A. Gavezzotti, Wiley, Chichester, U.K., 1997, pp. 61–97.
- 43 H. K. Buchholz, R. K. Hylton, J. G. Brandenburg, A. Seidel-Morgenstern, H. Lorenz, M. Stein and S. L. Price, *Cryst. Growth Des.*, 2017, **17**, 4676.
- 44 *CrystalExplorer17*, ed. M. J. Turner, J. J. McKinnon, S. K. Wolff, D. J. Grimwood, P. R. Spackman, D. Jayatilaka and M. A. Spackman, University of Western Australia, 2017, <http://hirshfeldsurface.net>.
- 45 S. Nunn and K. Nishikida, Thermo Fisher Scientific Application Note N° 50581, *Advanced ATR Correction Algorithm*, Madison, WI, USA, 2008.